Monthly Notices
of the
ROYAL ASTRONOMICAL SOCIETY

MNRAS **479,** 3604–3615 (2018)
Advance Access publication 2018 June 14

doi:10.1093/mnras/sty1558

Numerical modelling of tertiary tides

Yan Gao,[1,2]★ Alexandre C. M. Correia,[3,4,5] Peter P. Eggleton[6] and Zhanwen Han[1,2]

[1]*Yunnan Observatories, Chinese Academy of Sciences, Kunming 650011, China*
[2]*Key Laboratory for the Structure and Evolution of Celestial Objects, Chinese Academy of Sciences, Kunming 650011, China*
[3]*Department of Physics, University of Coimbra, P-3004-516 Coimbra, Portugal*
[4]*CIDMA, Department of Physics, University of Aveiro, P-3810-193 Aveiro, Portugal*
[5]*ASD, IMCCE, Paris Observatory, PSL University, 77 Av. Denfert-Rochereau, F-75014 Paris, France*
[6]*Lawrence Livermore National Laboratory, 7000 East Ave, Livermore, CA 94551, USA*

Accepted 2018 June 11. Received 2018 June 11; in original form 2018 April 20

ABSTRACT

Stellar systems consisting of multiple stars tend to undergo tidal interactions when the separations between the stars are short. While tidal phenomena have been extensively studied, a certain tidal effect exclusive to hierarchical triples (triples in which one component star has a much wider orbit than the others) has hardly received any attention, mainly due to its complexity and consequent resistance to being modelled. This tidal effect is the tidal perturbation of the tertiary by the inner binary, which in turn depletes orbital energy from the inner binary, causing the inner binary separation to shrink. In this paper, we develop a fully numerical simulation of these 'tertiary tides' by modifying established tidal models. We also provide general insight as to how close a hierarchical triple needs to be in order for such an effect to take place, and demonstrate that our simulations can effectively retrieve the orbital evolution for such systems. We conclude that tertiary tides are a significant factor in the evolution of close hierarchical triples, and strongly influence at least ∼1 per cent of all multiple star systems.

Key words: celestial mechanics – (stars:) binaries (including multiple): close – stars: evolution.

1 INTRODUCTION

Stars in close multiple systems are subject to tidal forces, which play a pivotal role in shaping their futures. The intrinsic mechanism behind these tidal forces is that, for every celestial body within a multiple system, the motion of the other bodies subjects it to a changing gravitational field, inducing internal motion within it, which in turn affects the gravitational field emanating from it, thereby influencing the rest of the system as a whole. In conjunction with dissipative processes (see Ogilvie 2014 for a review of such processes), tidal forces facilitate, among many other effects, the migration of angular momentum from one part of the system to another. Due to the importance of the various roles of these forces, previous studies have conducted extensive investigations about their nature.

Despite the relative simplicity of the concept, clarity has yet to be achieved as to exactly how tidal forces ought to be modelled. Some researchers (e.g. Hut 1981; Eggleton, Kiseleva & Hut 1998; Kiseleva, Eggleton & Mikkola 1998; Correia, Boué & Laskar 2016) favour a treatment based on equilibrium tides (usually referred to as the 'equilibrium tide model'), while others (e.g. Press & Teukolsky 1977; Mardling 1995a,b; Kumar & Goodman 1996; Correia et al. 2014; Ragazzo & Ruiz 2017) advocate a treatment that approximates the celestial body receiving the tidal force as an oscillator with many different oscillation modes, each one absorbing energy in its own way (known as the 'dynamical tide model'). It has been pointed out that the two models may be complementary (e.g. Eggleton et al. 1998), with each model being optimized for a special set of cases, but even so, it is still unclear where the line should be drawn when dealing with specific systems.

Yet however great the controversy may be when it comes to modelling tidal processes, there is a general consensus regarding the macroscopic effects of tidal forces; that they tend to synchronize the rotations and orbits of all the bodies involved, circularize orbits by causing a decay in their ellipticities, and convert certain portions of the kinetic and potential energies of the bodies involved into heat, which can then be radiated away. For instance, for a two-body system in a Keplerian orbit under tidal effects, given time, the system must ultimately evolve into a circular orbit, with the orbital angular velocity being equal to the respective rotational angular velocities of each body, regardless of how eccentric their initial orbit may be or how much their initial angular velocities may differ.

Of all the tidal effects to which close multiple systems are exposed, only three remain relevant for the orbital evolution of a hierarchical triple system (consisting of an inner binary of masses m_1 and m_2, as well as an outer tertiary of mass m_3). The first is the

★ E-mail: ygbcyy@ynao.ac.cn

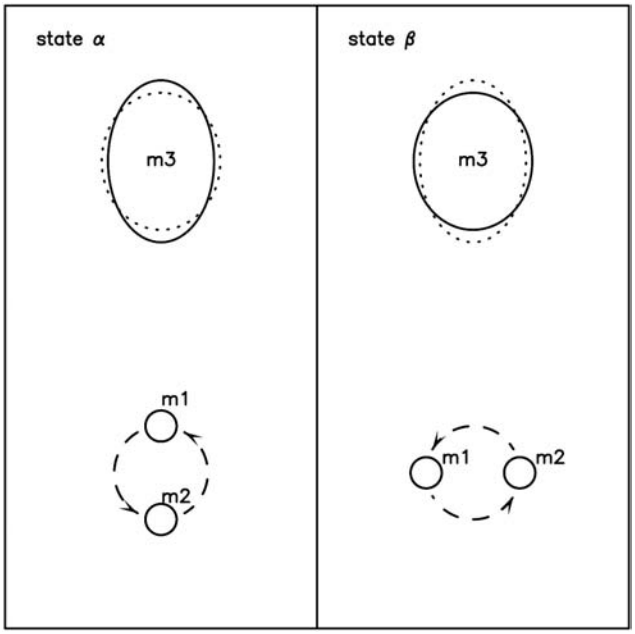

Figure 1. Illustration of how the inner binary affects the third body when tertiary tides become significant (see also the animated figure attached to this paper). The state when all three bodies are aligned, as depicted in the left-hand panel, is defined as state α, and the state in which the three bodies are at the vertices of an isosceles triangle, as depicted in the right-hand panel, is defined as state β. The solid lines display the shape of the tertiary at equilibrium tidal distortion, while the dotted lines represent the same shape in the other state for comparison. The tidal distortion of the tertiary is greatly exaggerated.

tidal locking between m_1 and m_2, which is no different from two-body tidal effects in general, and has historically been the subject of intense study (e.g. Counselman 1973; Hut 1981). The second is the tidal locking of m_3 to the inner binary, which will eventually synchronize the rotation and the orbit of m_3 (e.g. Correia et al. 2016). The third and final effect is the dumping of energy from m_1 and m_2 to m_3, which m_1 and m_2 achieve by tidally distorting m_3 as illustrated in the cartoon depiction in Fig. 1 (see also Animated Fig. 1).

As portrayed in Fig. 1, m_3 receives the greatest amount of tidal force from m_1 and m_2 when all three bodies are aligned (left-hand panel), and receives the least when they are orthogonal (right-hand panel). This change in received tidal force translates into a change in the degree of tidal distortion (elongation in the direction of m_1 and m_2) that m_3 undergoes. Consequently, if the internal tidal friction in m_3 is strong enough to (at least partly) brake the resultant internal motion, this leads to (at least part of) the energy carried in the tidal distortion difference being converted to heat. At whatever rate this process generates heat, it must essentially be fuelled by the orbital energy within the orbit of m_1 and m_2, which is the driving motion behind the tidal distortion of m_3. Therefore, this effect should serve also to drive the inner binary separation to be smaller. Here, it should be noted that these tidal effects will not end in tidal locking, as is often the case with two-body tidal effects, since no rotation of m_3 can decrease the difference in self-gravitational potential energy in the transition between the left-hand and right-hand panels of Fig. 1.

Of the three effects mentioned above, the first two have already been extensively investigated, as is evident from the literature. Very little attention, however, has been paid to the third. Admittedly, this is not entirely without good reason; in a vast majority of cases, m_3 is much smaller than its Roche lobe, and the tidal distortion it undergoes is consequently insignificant. However, whenever the condition comes to pass that m_3 is more or less the same size as its Roche lobe, this third effect becomes interesting for one simple reason: as mentioned above, this third effect can never be mitigated by tidal locking, and therefore can theoretically form an endless drain of the orbital energy of m_1 and m_2. Furthermore, we shall show that, unlike any other merger-contributing mechanism investigated so far, the greater the inner binary separation, the greater this energy drain per unit time will be. In other words, this effect is rare in that it preferentially allows large binary separations to decrease. So far, triple systems, in which m_3 is close enough for this third effect to have been prominent in the past, have occasionally been observed (e.g. Derekas et al. 2011). Speculation has also arisen that the inner binaries have been driven closer together due to three-body tidal effects, which are not inconsistent with observed properties of these triples (e.g. Fuller et al. 2013). However, there is not, to the knowledge of the authors, as of yet any work that provides a simulation that can recover the exact details of this third effect, and therefore the way in which the orbits of triple systems under its influence evolve is not well understood. We seek to remedy this.

For the rest of this paper, we shall refer to this third effect by the names 'tertiary tides' or 'TTs' for short. In what follows in this paper, we describe our model and its numerical implementation in Section 2, and present the results of our calculations for some specific systems in Section 3. Finally, our conclusions regarding the influence of tertiary tides in general, as well as the limitations of our work, are provided in Section 4, along with an extrapolation of what work could be done in the future.

2 TREATMENT OF TIDES AND TIDAL LAGS

To reliably simulate a close triple system undergoing TTs, we adopt a two-stage simulation based on eighth-order Runge Kutta methods (hereafter RK8), by modelling the orbital motion of three bodies in a hierarchical triple configuration. We treat the bodies constituting the inner binary m_1 and m_2 as point masses, whereas the third body m_3 is modelled as a body with a gravitational field varying with time, in order to account for its tidal distortion. In the first stage, we calculate the amount of energy extracted from the inner orbit per unit time, in which TTs are taken into account by means of a modified version of classical two-body tidal models (e.g. Counselman 1973; Zahn 1977, 2005; Hut 1981). For the second stage, we adopt a viscoelastic tidal model (e.g. Correia et al. 2014), calibrating an unknown parameter τ in this model by varying the parameter until the energy extraction rates of the two models match. This provides detailed positions and velocities of all three bodies, as well as the rotation and deformation of m_3, as a function of time. From these positions and velocities, orbital parameters (such as semimajor axes and periods) of both the inner and outer orbits can be retrieved. The details of each of these two stages are presented below.

2.1 Stage 1 simulations

We consider the special case of a hierarchical triple, consisting of a double point mass inner binary (m_1, m_2) in a circular orbit, and a coplanar third body (m_3), also in a circular orbit around the centre of mass (COM) of the inner binary (Jacobi coordinates). For simplicity, we assume that $m_1 = m_2$, and that m_3 is tidally locked to the inner binary's COM – in such a system, we do not consider rotational effects. Had it been the case that internal dissipation within m_3 was very efficient, the rate at which orbital energy is dumped from the

inner binary to m_3 can be shown to be

$$\frac{\mathrm{d}E}{\mathrm{d}t} \sim \frac{135}{4} \frac{Gm^2 R_3^5 a_1^2}{a_2^8} \frac{4}{P_{\rm in}}, \tag{1}$$

via a set of trivial calculations (see Appendix A for details). Here, $m = m_1 = m_2$, R_3 is the radius of m_3, a_1 and a_2 are the semimajor axes of the inner and outer orbits respectively, and $P_{\rm in}$ is the inner orbital period. However, since dissipation efficiency might be very low for this process (and we indeed find it to be so in our work), we need a much more detailed set of simulations, detailed below.

At each moment, m_3 has a proclivity to assume the distortion corresponding to the equilibrium tide of that particular moment. This equilibrium distortion at each moment leads to a gravitational field that can be approximately expressed by (see Appendix B)

$$V(r, \psi) = -\frac{Gm_3}{r} \left[1 + k_2 \zeta(\phi) \left(\frac{R_3}{r} \right)^2 P_2(\cos\psi) \right], \tag{2}$$

where k_2 is the Love number for m_3 (for polytropic stars with $n = 1.5$, we use $k_2 = 0.2$ as an approximation, following Yip & Leung 2017), r is the distance measured from the centre of m_3, the angle ψ is defined to be zero in the direction of the tertiary bulge maximum, and ζ is the tidal distortion parameter,

$$\zeta(\phi) = \left[\frac{P_2(\cos\psi_1)}{(r_1/a_2)^3} + \frac{P_2(\cos\psi_2)}{(r_2/a_2)^3} \right] \frac{m}{m_3} \left(\frac{R_3}{a_2} \right)^3, \tag{3}$$

where r_1 and r_2 are the distances from m_1 to m_3 and m_2 to m_3, respectively, ϕ is the angle between $\overrightarrow{m_1 m_2}$ and $\overrightarrow{m_3 C}$ (C being the COM of the inner binary), and ψ_1 and ψ_2 are the ψ values for m_1 and m_2, respectively. For circular orbits and $\alpha = a_1/a_2$,

$$\begin{aligned} \left(\frac{r_1}{a_2} \right)^3 &= \left(1 + \alpha\cos\phi + \frac{1}{4}\alpha^2 \right)^{3/2} \\ \left(\frac{r_2}{a_2} \right)^3 &= \left(1 - \alpha\cos\phi + \frac{1}{4}\alpha^2 \right)^{3/2} \end{aligned}. \tag{4}$$

Since internal dissipation is not instantaneous, the tertiary never achieves this equilibrium. Instead, it assumes some tidal distortion equivalent to its equilibrium state a certain amount of time $t_{\rm lag}$ ago, where $t_{\rm lag}$ is usually termed the tidal lag time.

But how much time is $t_{\rm lag}$? To answer this question, we draw an analogy from the $t_{\rm lag}$ in binary tidal locking. In a binary with component stars A and B (totally different from and irrelevant to the triple system mentioned above), where star A is an extended object that is not rotating, and star B is a point mass orbiting star A in a circular orbit at an angular velocity of ω, binary tidal locking occurs as follows. The existence of star B is supposed to distort star A at every epoch in a way such that star A is elongated in the direction of star B, forming two bulges on its surface, one pointing towards and the other away from star B, if equilibrium tides are assumed. However, since star A undergoes internal friction due to viscous processes, the orientation of those bulges always lags behind the orientation corresponding to equilibrium tide, or in other words, star A is constantly in a state of distortion corresponding to its tidal equilibrium a certain amount of time $t_{\rm lag}$ ago. Thus, the bulges are always aligned towards a position that star B was the same amount of time $t_{\rm lag}$ ago, corresponding to an angle λ away from B, thereby introducing a torque on the orbit of star B, decreasing its orbital angular momentum. Conversely, the rotational angular momentum of star A must increase due to conservation of angular momentum throughout the system.

It has been shown that $t_{\rm lag}$ can be expressed as

$$t_{\rm lag} = \frac{P}{2\pi}\lambda, \tag{5}$$

where P is the orbital period of the binary, and λ is the tidal lag angle, which can be expressed as (Zahn 1977, 2005)

$$\lambda = \omega t_{\rm dyn}^2 \left(\frac{1}{t_{\rm diss}} \right), \tag{6}$$

where $t_{\rm dyn}$ is the dynamical time-scale of star A, ω is the orbital angular velocity described above, and $t_{\rm diss}$ is the typical dissipation time-scale of star A. According to its definition, $t_{\rm dyn}$ is simply

$$t_{\rm dyn} = \sqrt{\frac{R^3}{GM}}. \tag{7}$$

The value of $t_{\rm diss}$, however, is a somewhat more complicated issue, and here we focus only on the aspects of its calculation immediately relevant to this paper. For a star with a convective envelope (which is the case for both low-mass main sequence stars and red giants), turbulent convection dominates the dissipation process for equilibrium tides (e.g. Zahn 2005), and $t_{\rm diss}$ is simply the convective time-scale $t_{\rm conv}$ when the tidal period (the period of variation of the tidal forcefield, which is also the orbital period in a two-body scenario) is longer than $t_{\rm conv}$:

$$t_{\rm diss} = t_{\rm conv} = \left(\frac{MR^2}{L} \right)^{1/3}, \tag{8}$$

where M, R, and L are the mass, radius and luminosity of star A, respectively. However, it is important to note that the above equation is only valid when the tidal forcefield changes very slowly, giving the perturbed body ample time to dissipate energy, as is the case when the tidal period is longer than $t_{\rm conv}$. When the tidal period is shorter than $t_{\rm conv}$, the perturbed body does not have sufficient time to dissipate this energy before the tidal forcefield reverts back to its former state, in which case a phenomenon called 'fast tides' starts to come into effect. When this happens, $t_{\rm diss}$ ought to be calculated via either

$$t_{\rm diss} = \left(\frac{t_{\rm conv}}{P} \right) t_{\rm conv}, \tag{9}$$

or

$$t_{\rm diss} = \left(\frac{t_{\rm conv}}{P} \right)^2 t_{\rm conv}, \tag{10}$$

or perhaps

$$t_{\rm diss} = \left(\frac{t_{\rm conv}}{P} \right)^{5/3} t_{\rm conv}, \tag{11}$$

according to Zahn (2005), Goldreich & Keeley (1977), and Goodman & Oh (1997), respectively. It is not currently known which, if any at all, of these treatments approximates fast tides well (e.g. Ogilvie 2014; Mathis et al. 2016), but recent results seem to favour the first prescription for stellar interiors (Penev et al. 2007, 2009), and hence we will use this prescription for our following calculations.

Having found a way to calculate $t_{\rm lag}$ for binary tides, we return to our previous triple system with m_1, m_2, and m_3. The method above can be converted into a calculation for $t_{\rm lag}$ in TTs as shown below.

The tidal distortion of m_3 experienced during TTs depicted in Fig. 1 is a combination of separate tidal distortions by m_1 and m_2 (see Fig. 2 for an illustration of a single component). Since $m_1 = m_2$, and considering the general symmetry of the inner binary, the

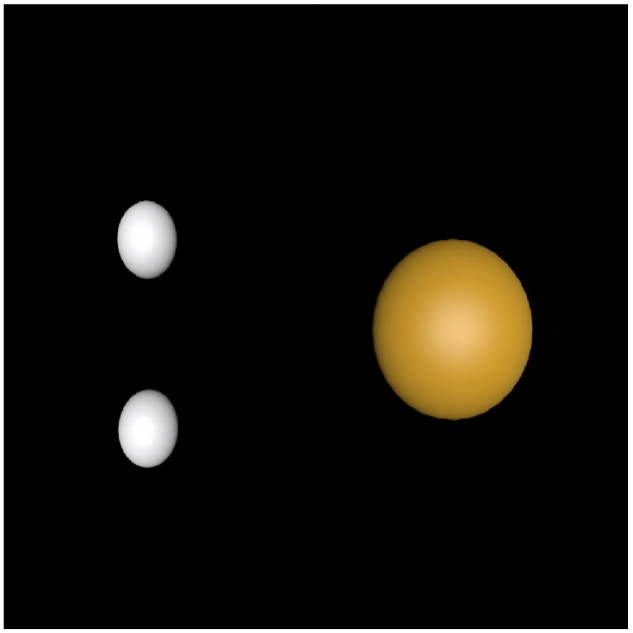

Figure 2. Dissection of tertiary tides – how the tertiary is tidally distorted in reaction to the tidal forcing from one component of the inner binary alone. Here, the effects of the other component of the inner binary have been eliminated, but its companion is assumed to travel in the same orbit as before. The solid lines display the shape of the tertiary at equilibrium tidal distortion, while the dotted lines represent its shape when no tidal forces are applied. The dash-dotted lines indicate the direction of elongation of the equilibrium tide distortion, which is invariably in the direction of the perturbing body. The time given in the upper left corner of each panel is given in units of inner binary orbital period. It can be seen that the net result is an oscillatory rotational effect, but this rotation is largely cancelled out by the effects of the other inner binary component when full tertiary tides are considered. The tidal distortion of the tertiary is greatly exaggerated.

$t_{\rm lag}$ of the distortion caused by m_1 must be equal to that caused by m_2. Hence, we only need to calculate the value of $t_{\rm lag}$ due to either m_1 or m_2 in order to retrieve the $t_{\rm lag}$ for the tidal distortion of m_3.

How, then, should this $t_{\rm lag}$ be calculated, and how long is it for the triple system in question? To answer this, we revert to the calculation of the tidal lag time in a binary system, as presented in equations (5) and (6). For our TTs, the tertiary lag time should also be calculated with these equations, albeit with minor modifications as to what physical quantities each of the variables correspond to in a triple system under TTs. The dynamical time-scale $t_{\rm dyn}$ is indisputably the dynamical time-scale of the tertiary, but for the other variables, namely P, ω, and $t_{\rm diss}$, it may not be so obvious.

To find what value to substitute for P, one must discern exactly what P is in equation (5). Considering that λ is simply the tidal lag angle, and hence whatever remains is merely a conversion factor from lag angle to lag time, it becomes clear that P is more related to how the perturbing body is moving relative to the perturbed body than it is to the intrinsic period of the acting tidal force. In other words, it would not matter at any particular moment if the perturbing body were travelling in a circular orbit, or in a straight line tangential to that circular orbit, and had happened to be at the point of intersection at that particular moment – both scenarios would result in the same $t_{\rm lag}$, had the lag angle been the same. In fact, equations (5) and (6) could be more accurately expressed as

$$t_{\rm lag} = \frac{d}{v}\left(\omega t_{\rm dyn}^2 \frac{1}{t_{\rm diss}}\right), \tag{12}$$

where d is the distance between the perturbed body and its companion, and v is the relative velocity between the two bodies. To extrapolate this to tertiary tides, it may be beneficial to imagine the moment when the inner binaries are in state α of Fig. 1 (left-hand panel). Assuming that the tertiary is not rotating relative to the inner binary, and considering that $a_2 \gg a_1$, one can see that, at this moment, d should be substituted by a_2, and v by the inner orbital velocity (the velocity at which m_1 and m_2 move relative to their COM), hereby denoted as $v_{\rm in}$. At moments when the triple system is not in state α, the calculation of what values to substitute will be more problematic (possibly starting with the second term in equation (12) of Kiseleva et al. 1998), and is beyond the scope of this paper. For the purposes of this study, we assume that $t_{\rm lag}$ is the same at all epochs, and hence we use $d = a_2$, $v = v_{\rm in}$ for all epochs, which is equivalent to

$$P = \frac{2\pi a_2}{v_{\rm in}}. \tag{13}$$

The ω in equation (6) is a measure of the lack of synchronism between the rotation of the perturbed body and its companion's orbit, and is therefore a function of the periodical variation of the tidal force acting upon the perturbed body. Thus, for tertiary tides, we set

$$\omega = 2\pi\left(\frac{1}{P_{\rm in}} - \frac{1}{P_{\rm rot}}\right) = 2\pi\left(\frac{1}{P_{\rm in}} - \frac{1}{P_{\rm out}}\right) \approx \frac{2\pi}{P_{\rm in}}, \tag{14}$$

where $P_{\rm in}$ is the orbital period of the inner binary, $P_{\rm rot}$ is the rotational period of m_3, which we assume in our Stage 1 simulations to be equal to the outer orbital period $P_{\rm out}$ due to tidal locking.

As for the dissipation time-scale $t_{\rm diss}$, since the tidal period is equal to $P_{\rm in}$, which is consistently greater than the convective time-scale $t_{\rm conv}$ for all cases of TTs we consider, $t_{\rm diss}$ needs to be calculated via a prescription for fast tides, for which we use equation (9), and therefore

$$t_{\rm diss} = \frac{t_{\rm conv}^2}{P_{\rm in}}, \tag{15}$$

where $t_{\rm conv}$ can be calculated, as with any normal star, via equation (8) above.

Having ascertained the value of $t_{\rm lag}$, we then proceed with three sets of simulations to calculate the rate at which TTs extract orbital energy.

In the first set, we run a simulation where m_1, m_2, and m_3 are all treated as point masses by solving the following set of equations using eighth-order Runge–Kutta:

$$\frac{{\rm d}\boldsymbol{v}_{\rm i}}{{\rm d}t} = \frac{Gm_{\rm j}}{r_{\rm ij}^3}(\boldsymbol{R}_{\rm j} - \boldsymbol{R}_{\rm i}) + \frac{Gm_{\rm k}}{r_{\rm ik}^3}(\boldsymbol{R}_{\rm k} - \boldsymbol{R}_{\rm i}), \tag{16}$$

where blackfont denotes vectors, $\boldsymbol{R}_{\rm i}$ is the position vector of $m_{\rm i}$, i = (1,2,3), j = (2,1,1), and k = (3,3,2). This is done to check that the triple system is dynamically stable without the effects of tidal forces, and also serves to establish a baseline for the errors incurred during the simulations.

In the second set, we run a three-body simulation as before, but modulate the gravitational field of m_3 according to equation (2) with a giant tertiary (large radius) and a tidal lag. The lag is implemented by letting ζ at each timestep be what its equilibrium value would

have been $t_{\rm lag}$ ago. In other words,

$$\begin{aligned}
\frac{\mathrm{d}\boldsymbol{v}_1}{\mathrm{d}t} &= \frac{Gm_2}{r_{12}^3}(\boldsymbol{R}_2-\boldsymbol{R}_1)-\frac{V\,(r_{13},\psi_1)}{r_{13}^2}(\boldsymbol{R}_3-\boldsymbol{R}_1),\\
\frac{\mathrm{d}\boldsymbol{v}_2}{\mathrm{d}t} &= \frac{Gm_1}{r_{21}^3}(\boldsymbol{R}_1-\boldsymbol{R}_2)-\frac{V\,(r_{23},\psi_2)}{r_{23}^2}(\boldsymbol{R}_3-\boldsymbol{R}_2),\\
\frac{\mathrm{d}\boldsymbol{v}_3}{\mathrm{d}t} &= \frac{Gm_1}{r_{31}^3}(\boldsymbol{R}_1-\boldsymbol{R}_3)+\frac{Gm_2}{r_{32}^3}(\boldsymbol{R}_2-\boldsymbol{R}_3),
\end{aligned} \tag{17}$$

where the gravitational potential function $V(r, \psi)$ is given by equation (2), and the value of ζ in the function is given as the equilibrium tide value $t_{\rm lag}$ ago. This is done to check that the triple system is dynamically stable after TTs are applied, and that the distortions of m_3 will not disintegrate the system before TTs come into effect. Theoretically, the energy extraction rate can be found using this method, but the errors induced by our approximations are larger than the benchmark set by our first set of simulations, and therefore we need another set of simulations to find this extraction rate.

In the third set of simulations, we model the inner binary orbit only, adding an additional varying gravitational field centred at a distance a_2 from the COM of the inner binary. This field is equivalent to the effect of an m_3 tidally distorted by the orbiting inner binary, minus an m_3 tidally distorted by a point mass of $m_1 + m_2$. The tidal lags are dealt with as before. The effective equations for this set of simulations are

$$\begin{aligned}
\frac{\mathrm{d}\boldsymbol{v}_1}{\mathrm{d}t} &= \frac{Gm_2}{r_{12}^3}(\boldsymbol{R}_2-\boldsymbol{R}_1)+k_2\left(\zeta\,(\phi)-\zeta_{\rm eq}\right)\\
&\quad\left(\frac{R_3}{a_2}\right)^2 P_2(\cos\psi_1)\frac{Gm_3}{r_{13}^3}(\boldsymbol{R}_3-\boldsymbol{R}_1),\\
\frac{\mathrm{d}\boldsymbol{v}_2}{\mathrm{d}t} &= \frac{Gm_1}{r_{21}^3}(\boldsymbol{R}_1-\boldsymbol{R}_2)+k_2\left(\zeta\,(\phi)-\zeta_{\rm eq}\right)\\
&\quad\left(\frac{R_3}{a_2}\right)^2 P_2(\cos\psi_2)\frac{Gm_3}{r_{23}^3}(\boldsymbol{R}_3-\boldsymbol{R}_2)\\
\boldsymbol{v}_3 &= \frac{\boldsymbol{v}_1+\boldsymbol{v}_2}{2}.
\end{aligned} \tag{18}$$

Here,

$$\zeta_{\rm eq}=\frac{(m_1+m_2)}{m_3}\left(\frac{R_3}{a_2}\right)^3 \tag{19}$$

is the ζ value for an m_3 perturbed by a point mass of $m_1 + m_2$ at the COM of the inner binary, and tidal lags are applied via $\zeta(\phi)$ as in the second set. This excludes all effects other than TTs, and yields the rate of energy extraction, with which we then use to calibrate τ in our Stage 2 simulations (see below), by varying τ until the energy extraction rate matches that given by this model.

2.2 Stage 2 simulations

While our Stage 1 simulations can provide the rate at which TTs extract energy from the inner binary, some details of the process (such as the rotation of the tertiary) are lost in the approximations. For a more convincing picture of how a hierarchical triple behaves under TTs, we resort to the following model.

Again, we consider the previous hierarchical coplanar triple system consisting of three stars with masses m_1, m_2, and m_3. As before, m_1 and m_2 are considered to be point masses, while the tertiary is considered to be an oblate ellipsoid with mean radius R_3 and gravity field coefficients J_2, C_{22}, and S_{22}, sustained by the reference frame $(\boldsymbol{I}, \boldsymbol{J}, \boldsymbol{K})$, where $\boldsymbol{K}$ is the axis of maximal inertia. We furthermore assume that the spin axis of the tertiary, with rotation rate Ω, is also along $\boldsymbol{K}$, and that $\boldsymbol{K}$ is orthogonal to the orbital plane (which corresponds to zero obliquity). The gravitational potential of the tertiary is then given by (e.g. Correia & Rodríguez 2013):

$$\begin{aligned}
V(\boldsymbol{r}) = &-\frac{Gm_3}{r}-\frac{Gm_3R_3^2J_2}{2r^3}\\
&-\frac{3Gm_3R_3^2}{r^3}\left(C_{22}\cos 2\gamma - S_{22}\sin 2\gamma\right),
\end{aligned} \tag{20}$$

where

$$\cos 2\gamma = (\boldsymbol{I}\cdot\hat{\boldsymbol{r}})^2-(\boldsymbol{J}\cdot\hat{\boldsymbol{r}})^2 \quad\text{and}\quad \sin 2\gamma = -2(\boldsymbol{I}\cdot\hat{\boldsymbol{r}})(\boldsymbol{J}\cdot\hat{\boldsymbol{r}}) \tag{21}$$

where $\boldsymbol{r}$ is a generic position with respect to the centre of the tertiary, and $\hat{\boldsymbol{r}} = \boldsymbol{r}/r$ is the unit vector. We neglect terms in $(R_3/r)^3$ (quadrupolar approximation). We can also express $\gamma = \theta - f$, where θ is the rotation angle, and f is the true longitude. The total potential energy of the system is thus given by

$$U(\boldsymbol{r}_1,\boldsymbol{r}_2) = -\frac{Gm_1m_2}{|\boldsymbol{r}_2-\boldsymbol{r}_1|}+m_1V(\boldsymbol{r}_1)+m_2V(\boldsymbol{r}_2)\,,\,, \tag{22}$$

where $\boldsymbol{r}_i = \boldsymbol{R}_i - \boldsymbol{R}_3$, and $\boldsymbol{R}_i$ is the position of the star with mass m_i in an inertial frame. Note that the quantities a_1 and a_2 (Jacobi coordinates) are not the norms of $\boldsymbol{r}_1$ and $\boldsymbol{r}_2$, which are astrocentric coordinates (see Appendix B for more details).

The equations of motion governing the orbital evolution of the system in an inertial frame are given by:

$$\frac{\mathrm{d}^2\boldsymbol{R}_i}{\mathrm{d}t^2} = -\frac{1}{m_i}\frac{\partial U}{\partial \boldsymbol{R}_i} = -\frac{1}{m_i}\frac{\partial U}{\partial \boldsymbol{r}_i} \tag{23}$$

$$\frac{\mathrm{d}^2\boldsymbol{R}_3}{\mathrm{d}t^2} = -\frac{1}{m_3}\frac{\partial U}{\partial \boldsymbol{R}_3} = \frac{1}{m_3}\left(\frac{\partial U}{\partial \boldsymbol{r}_1}+\frac{\partial U}{\partial \boldsymbol{r}_2}\right) \tag{24}$$

with

$$\begin{aligned}
\frac{\partial U}{\partial \boldsymbol{r}_i} = &(-1)^i\frac{Gm_1m_2}{|\boldsymbol{r}_2-\boldsymbol{r}_1|^3}(\boldsymbol{r}_2-\boldsymbol{r}_1)+\frac{Gm_im_3}{r_i^3}\boldsymbol{r}_i\\
&+\frac{3Gm_im_3R_3^2}{2r_i^5}\left[J_2+6\left(C_{22}\cos 2\gamma_i - S_{22}\sin 2\gamma_i\right)\right]\boldsymbol{r}_i\\
&-\frac{6Gm_im_3R_3^2}{r_i^5}\left(C_{22}\sin 2\gamma_i + S_{22}\cos 2\gamma_i\right)\boldsymbol{K}\times\boldsymbol{r}_i.
\end{aligned} \tag{25}$$

In an astrocentric frame they simply become

$$\frac{\mathrm{d}^2\boldsymbol{r}_i}{\mathrm{d}t^2} = -\left(\frac{1}{m_i}+\frac{1}{m_3}\right)\frac{\partial U}{\partial \boldsymbol{r}_i}-\frac{1}{m_3}\frac{\partial U}{\partial \boldsymbol{r}_j} \tag{26}$$

where $i = 1, 2$, and $j = 3 - i$.

The torque acting to modify the rotation of the tertiary is given by

$$I_3\frac{\mathrm{d}\Omega}{\mathrm{d}t} = \left(\boldsymbol{r}_1\times\frac{\partial U}{\partial \boldsymbol{r}_1}+\boldsymbol{r}_2\times\frac{\partial U}{\partial \boldsymbol{r}_2}\right)\cdot\boldsymbol{K} \tag{27}$$

for a tertiary of constant radius, where I_3 is the principal moment of inertia of m_3 along the axis $\boldsymbol{K}$. We hence obtain for the rotation angle $\dot{\theta} = \Omega$:

$$\begin{aligned}
\frac{\mathrm{d}^2\theta}{\mathrm{d}t^2} = &-\frac{6Gm_1m_3R_3^2}{I_3r_1^3}\left[C_{22}\sin 2\gamma_1 + S_{22}\cos 2\gamma_1\right]\\
&-\frac{6Gm_2m_3R_3^2}{I_3r_2^3}\left[C_{22}\sin 2\gamma_2 + S_{22}\cos 2\gamma_2\right]\,.
\end{aligned} \tag{28}$$

For a tertiary with varying radius, the above equation becomes

$$\frac{\mathrm{d}^2\theta}{\mathrm{d}t^2} = -2\Omega\frac{\dot{R}_3}{R_3} - \frac{6Gm_1m_3R_3^2}{I_3r_1^3}\left[C_{22}\sin 2\gamma_1 + S_{22}\cos 2\gamma_1\right] - \frac{6Gm_2m_3R_3^2}{I_3r_2^3}\left[C_{22}\sin 2\gamma_2 + S_{22}\cos 2\gamma_2\right] . \quad (29)$$

When this is the case, we find a discrete $R_3 = R_3(t)$ via stellar evolution codes and use cubic spline interpolation to determine both R_3 and $\mathrm{d}R_3/\mathrm{d}t$ at each epoch.

The tertiary is deformed under the action of self-rotation and tides. Therefore, the gravity field coefficients can change with time as the shape of the tertiary is continuously adapting to the equilibrium figure. According to the Maxwell viscoelastic rheology, the deformation law for these coefficients is given by (e.g. Correia et al. 2014):

$$\begin{aligned} J_2 + \tau\dot{J}_2 &= J_2^r + J_2^t \\ C_{22} + \tau\dot{C}_{22} &= C_{22}^t \\ S_{22} + \tau\dot{S}_{22} &= S_{22}^t , \end{aligned} \quad (30)$$

where

$$J_2^r = k_2\frac{\Omega^2R_3^3}{3Gm_3} \quad (31)$$

is the rotational deformation, and

$$\begin{aligned} J_2^t &= k_2\frac{m_1}{2m_3}\left(\frac{R_3}{r_1}\right)^3 + k_2\frac{m_2}{2m_3}\left(\frac{R_3}{r_2}\right)^3 \\ C_{22}^t &= \frac{k_2}{4}\frac{m_1}{m_3}\left(\frac{R_3}{r_1}\right)^3\cos 2\gamma_1 + \frac{k_2}{4}\frac{m_2}{m_3}\left(\frac{R_3}{r_2}\right)^3\cos 2\gamma_2 \\ S_{22}^t &= -\frac{k_2}{4}\frac{m_1}{m_3}\left(\frac{R_3}{r_1}\right)^3\sin 2\gamma_1 - \frac{k_2}{4}\frac{m_2}{m_3}\left(\frac{R_3}{r_2}\right)^3\sin 2\gamma_2 \end{aligned} \quad (32)$$

are the tidal equilibrium values for the gravity coefficients, and τ is the relaxation time of the tertiary in response to deformation. Usually, $\tau = \tau_\mathrm{v} + \tau_\mathrm{e}$, where τ_v and τ_e are the viscous (or fluid) and Maxwell (or elastic) relaxation times, respectively. However, for simplicity, we consider $\tau_\mathrm{e} = 0$, since this term does not contribute to the tidal dissipation (see Correia et al. 2014). This τ is the previously mentioned unknown parameter calibrated using our Stage 1 simulations. For an evolving tertiary, τ admittedly changes with time, but its degree of variation is not prominent enough to warrant treating it as a variable, for the purposes of the simulations mentioned in this paper.

3 EXAMPLES OF SYSTEMS UNDERGOING TTS

To showcase the effects of TTs, as well as the capabilities of our simulations, we run two sets of simulations: one for a purely hypothetical system consisting of two white dwarfs (WDs) and a main sequence (MS) star, with orbital parameters designed to maximize TTs, and the other for an observed multiple star system, namely HD97131. This section provides the details of these systems, as well as our results.

3.1 Hypothetical scenario

Here, we consider a purely hypothetical hierarchical triple, in which the inner binary consists of a pair of tidally locked WDs, and the tertiary is an MS star, tidally locked to the inner binary's COM. The masses are given as $m_1 = m_2 = 0.8\ \mathrm{M}_\odot$, $m_3 = 1.6\ \mathrm{M}_\odot$, and the orbital semimajor axes as $a_1 = 0.2$ AU, $a_2 = 2$ AU. The orbits are set to be coplanar and prograde, and all orbits are given to be circular. In this system, the WDs can readily be approximated as point masses, thus forming a ripe testing ground for tertiary tides. It should be noted that its circular and coplanar orbits also preclude Lidov–Kozai Resonance (Kozai 1962; Lidov 1962) from this system.

Table 1. Initial parameters for our second-stage simulations in the tertiary RGB phase for both our hypothetical scenario and HD97131.

Parameter	Hypothetical scenario	HD97131
a_1/AU	0.2	0.0373
a_2/AU	2.0	0.7955
e_1	0	0
e_2	0	0.191
$m_1/\mathrm{M}_\odot$	0.8	1.29
$m_2/\mathrm{M}_\odot$	0.8	0.90
$m_3/\mathrm{M}_\odot$	1.6	1.50
τ/yr	0.534	0.019

There are two main reasons why we choose such a system for our demonstration. The first is that this system is realistic – with an inner orbit of 25.8 d and an outer orbit of 577.4 d, this system has similar orbital periods to triple systems that have actually been observed. In fact, extensive studies by Tokovinin (1997) have found many triple systems with inner and outer orbital periods close to and straddling these (see their fig. 3). The second is that this system is stable according to conventional wisdom, if all three bodies were point masses. Adopting the methods and criteria of Musielak et al. (2005), we check this by following the dynamical evolution of the system over 4000 outer orbits using RK8, and examining their trajectories. The orbits are found to be stable, which is expected, given that the system falls within well-established stable zones (e.g. Musielak et al. 2005; Cuntz 2014).

Using our two-stage simulation method, we find that the effect of TTs is negligible when m_3 is still an MS star. This is expected, since the radius of a 1.6 $\mathrm{M}_\odot$ MS star is relatively small (about 1 $\mathrm{R}_\odot$), whereas tidal phenomena typically require radii on the order of the Roche lobes of the systems involved. However, MS stars evolve into red giants later in their lifetimes, and red giants have much larger radii. Using well-established stellar evolution algorithms (Eggleton 1973; Pols et al. 1995; Paxton et al. 2011), we find that a 1.6 $\mathrm{M}_\odot$ star stays in the red giant phase for many Myrs, during which its radius expands to more than 140 solar radii. This radius is close to, but just short of, its Roche lobe, and therefore we need not consider the effects of Roche lobe overflow.

Again adopting our two-stage simulation method, and assuming a constant radius of 100 solar radii for m_3, we retrieve a τ of 0.534 yr (see Table 1), and find that the inner binary orbit shrinks significantly within just a few Myrs due to TTs alone (Fig. 3). Throughout the inner binary orbital shrinkage, angular momentum from the inner orbit is transferred to the outer orbit, and a_2 marginally increases as a result, though not enough to shut down further shrinkage of a_1 due to TTs.

We also find that, after m_3 becomes a red giant, its rotational velocity is never exactly locked to the inner binary, even though the deviation is small. This is probably due to the fact that, for a perfectly locked m_3, the mass elements of m_3 that are closer to the inner binary will have a tendency to move in the same direction as the closer inner binary component, thereby inducing a rotation that deviates from a perfectly tidally locked scenario. While this

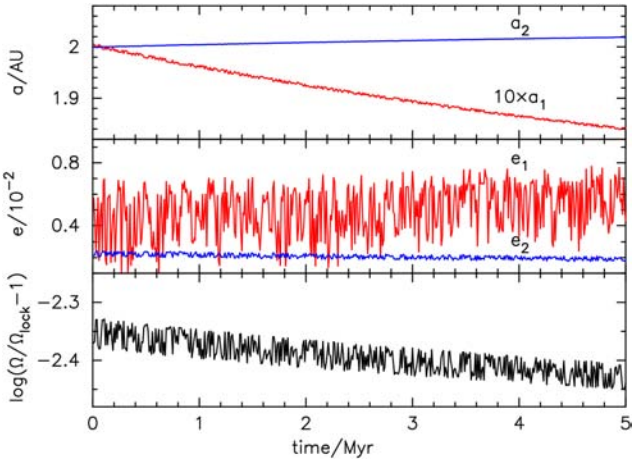

Figure 3. Orbital evolution of a hierarchical triple with $m_1 = m_2 = 0.8\,M_\odot$, $m_3 = 1.6\,M_\odot$, $a_1 = 0.2$ AU, $a_2 = 2$ AU, $e_1 = e_2 = 0$, and a constant tertiary radius of 100 solar radii. The inner binary orbit shrinks significantly within just a few Myrs due to TTs alone, while other orbital parameters also undergo some evolution. The rotational velocity of m_3 deviates from being perfectly tidally locked with the inner binary by a small amount, due to reasons explained in the text.

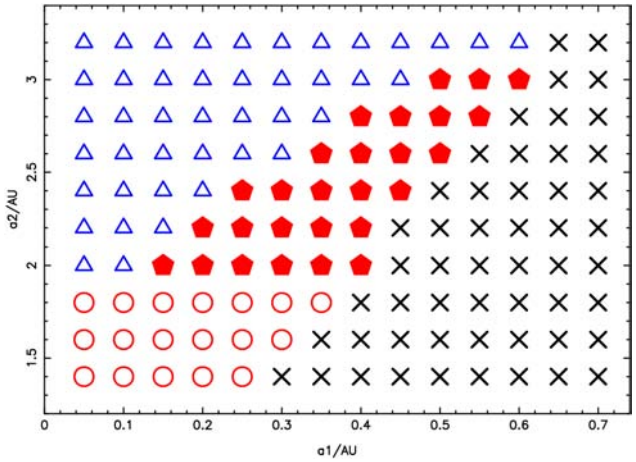

Figure 4. Prominence of tertiary tides in $a_1 - a_2$ space for our hypothetical hierarchical triple system with $m_1 = m_2 = 0.8\,M_\odot$, $m_3 = 1.6\,M_\odot$, all orbits being coplanar and circular. The black crosses indicate the region in which a_2/a_1 is too small, and the system is dynamically unstable; the blue triangles cover the region in which a_2 is too large, and TTs have no noticeable effect; the red circles represent areas where m_3 would fill its Roche lobe, in which Roche lobe overflow will compete with TTs for dominance. Only in the region with the filled red pentagons are TTs the exclusive dominating factor in merging the binary.

deviation is unlikely to be of much physical significance in our model, calculations pertaining to tidal effects in close triple systems, performed with models of dynamical oscillation modes under the assumption of perfect tidal locking, may require special attention in this regard.

But what if the inner or outer orbital separations in the triple system were larger or smaller? After all, realistic triple systems have a great range of values for a_1 and a_2. To check the separation dependence of TTs, we conduct a grid of first-stage simulations in $a_1 - a_2$ space for the same $m_1 = m_2 = 0.8\,M_\odot$, $m_3 = 1.6\,M_\odot$ system, and check how fast TTs can remove orbital energy from the inner binary for each set of (a_1, a_2). The conclusion is that, for different sets of (a_1, a_2), one of four different scenarios are possible: (i) if a_2/a_1 is too small, the system is dynamically unstable, and the orbits will evolve unpredictably whether TTs are considered or not; (ii) if a_2 is too large, TTs will have no noticeable effect; (iii) if a_2 is too small, m_3 will fill its Roche lobe at some point during its evolution. While this does not invalidate the influence of TTs (TTs can lead to very significant orbital shrinkage of the inner binary before Roche lobe overflow even begins, as demonstrated later in this section), it does lead to complications as to which effect dominates the evolution of the binary thereafter, which are beyond the scope of this paper; (iv) only in a triangular region straddled by these three regions are TTs the exclusive dominating factor. We plot these four regions in $a_1 - a_2$ space for our $m_1 = m_2 = 0.8\,M_\odot$, $m_3 = 1.6\,M_\odot$ system (Fig. 4). It can be seen that it is only in some of the closest hierarchical triples that TTs play a dominant role.

3.2 HD97131

How would TTs influence a realistic hierarchical triple system? To answer this question, we refer ourselves to the real-world hierarchical triple HD97131. HD97131 is a coplanar triple system (Torres et al. 2003) with m_3 being an MS star of spectral type F0. The inner orbit (between m_1 and m_2) is circular, while the outer orbit (which we assume to be prograde) has an eccentricity of $e_2 = 0.191$. The other relevant orbital parameters are $m_1 = 1.29\,M_\odot$, $m_2 = 0.90\,M_\odot$, $m_3 = 1.50\,M_\odot$, $a_1 = 0.0373$ AU, and $a_2 = 0.7955$ AU (Tokovinin 1997, 2008). At such a small a_2, the Roche lobe for m_3 is small, only 57.1 solar radii (Eggleton 1983). Thus, m_3 will inevitably fill its Roche lobe during its red giant phase . However, since the effects of Roche lobe mass transfer do not become significant until after its onset, this fact will not affect our analysis of TTs, which will shrink a_1 long before this happens. Unlike our previous simulation, we account for the radius evolution of m_3 by calculating the radius as a function of time using the aforementioned stellar evolution codes (Eggleton 1973; Pols et al. 1995; Paxton et al. 2011), and performing a cubic spline interpolation on the results. For our following simulations, we use the final 4.8 Myrs of the radius evolution of m_3 up to 1 Myr after Roche lobe overflow. This means that our simulation starts with the initial orbital parameters, but with m_3 already well into its red giant branch (RGB) phase, and filling its Roche lobe at t =3.8 Myrs.

To simulate HD97131, we use our two-stage method described in Section 2. However, since many of the assumptions regarding our first-stage simulations break down for systems with $m_1 \neq m_2$ and $e_2 \neq 0$, we make the following modifications to our methods. For our first-stage simulations, we set the masses of both inner binary components to $\frac{m_1+m_2}{2}$, and set the tertiary in a circular orbit with a semimajor axis of $a_2(1 - e_2^2)$. The justification for the latter is that, assuming conservation of angular momentum, the semimajor axis of the outer orbit will evolve to that particular value if the orbit was to be tidally circularized. Our results show that this is indeed the case. With these modifications to the system, our original assumptions hold, and the first-stage simulations can be conducted. While this leads to a first stage simulation of a system somewhat different from the actual HD97131, this difference is not important, as our first stage simulations are only used to calibrate the value of τ for our second-stage simulations, which are responsible for the recovery of exact details of the orbital evolution. We find a τ of 0.019 yr. For the second-stage simulations, we use the orbital parameters of the actual HD97131 (as documented in Table 1).

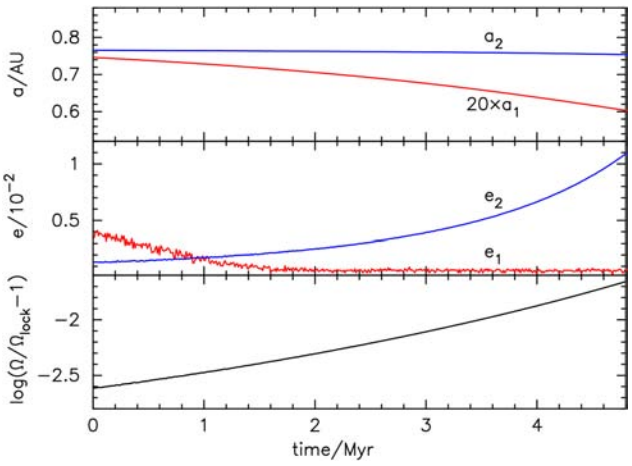

Figure 5. Projected orbital evolution for HD97131, after its tertiary becomes a red giant. It can be seen that the inner orbital separation a_1 decreases significantly due to TTs, while the evolution of the outer orbital separation a_2 is negligible. The evolution of the orbital eccentricities is evident, as is that of Ω, the rotation of m_3. Note that the initial $e_2 = 0.191$ vanishes in just a few thousand years, and is consequently not visible in this plot. Ω evolves to deviate from the tidally locked value as expected, due to reasons explained in the paper.

Tracing the orbital evolution of HD97131 during the red giant phase of m_3, we find that the outer orbit is rapidly circularized, reducing e_2 to less than 0.01 in just a few thousand years. This is expected (e.g. Correia et al. 2016), and will therefore warrant no further attention here. Thereafter, the inner binary orbit shrinks as witnessed in our previous simulations, with some minor evolution of the other orbital parameters (Fig. 5). It should be noted that the GW merging time-scale of the inner binary is brought down to less than half its original value during this process (see Peters 1964). The slight deviation from exact tidal locking in the rotation of m_3 is again seen.

4 DISCUSSION

Our results unequivocally show that TTs have a profound impact on very close hierarchical triples. While it is evident that this translates into a negligible effect when considering stellar populations in general, our understanding of certain exotic systems can be spurious if it were to be neglected altogether.

For starters, gravitational wave (GW) mergers (e.g. Abbott et al. 2016) require very close massive objects as progenitors. It is also well known that multiplicity is enhanced in stellar objects of such masses (e.g. Sana et al. 2012), and that GW mergers can arise from multiple interactions in globular clusters (e.g. Rodriguez et al. 2016). In both of these cases, TTs will be much more prevalent than in any general stellar population, though it is difficult to be certain by how much.

Of the many possible sources (e.g. Whelan & Iben 1973; Webbink 1984; Han & Podsiadlowski 2004; Pakmor et al. 2013) of Type Ia supernovae (SNe Ia for short), one proposed progenitor system involving three-body interactions has received a certain degree of attention in recent years (Fabrycky & Tremaine 2007; Thompson 2011; Shappee & Thompson 2013; Dong et al. 2015), despite the fact that it is unlikely to be one of the main sources of SN Ia production (Hamers et al. 2013). In these systems, the existence of a tertiary drives a WD binary into a merger or collision, by means of Lidov–Kozai oscillations. While Lidov–Kozai oscillations are less diminished by large values of a_2 than are TTs, it is conceivable that such systems preferably have small values of a_2, and therefore at least some of these systems must be susceptible to TTs. Furthermore, Lidov–Kozai oscillations are only an issue when mutual inclinations between the inner and outer orbits are high (∼40 deg or more), whereas TTs work for both coplanar and highly inclined systems. Thus, SN Ia production rates from such progenitor systems will be underestimated, should TTs be left unaccounted for. Another analogous issue is the enrichment in the high-mass end of WD mass functions (e.g. Rebassa-Mansergas et al. 2015), which cannot be explained by WD mergers via gravitational waves alone. While TTs are unlikely to have contributed significantly to this enrichment, they could potentially amplify the rate of WD mergers if WD binaries are found to have a greater degree of multiplicity than previously thought.

Last but not least, there have been attempts to explain observational phenomena with models of binary mergers occurring inside the envelopes of giant stars (e.g. Hillel, Schreier & Soker 2017). Should such studies ever reach the point where a detailed simulation of a progenitor system is required, TTs must be considered, as any binary must undergo a phase of non-negligible TTs before it can end up inside the envelope of a giant star.

In summary, TTs should play a pivotal role in the orbital evolution of certain systems. This role is even more preponderant when one considers the fact that a smaller a_1 can further exacerbate other mechanisms that drive the inner binary closer together (e.g. gravitational waves). The only limiting factor of their general influence on three-body evolution is the fraction of systems that will experience significant TTs; as of yet, observational evidence of how frequently they occur is not available. An examination of observed triple systems (Tokovinin 1997, 2008) seems to imply that only a very small fraction (∼1 per cent) will undergo significant TTs in the future; however, since TTs and other effects that act in close triples have a tendency to destroy their host systems, resulting in them ending up as binaries, not to mention observational biases that may limit the amount of very close triples seen, it is fairly hard to say what fraction of triples would be influenced by future TTs at the time of their birth. Perhaps the best way to ascertain this would be to collect samples of hierarchical triples in which the tertiaries are stars that have already evolved beyond their red giant phases, and to compare their a_1 values against those of triples with less advanced tertiaries; such observations of post-red giant tertiaries, however, are currently rare. Opportunities to directly observe TTs in action may present themselves from time to time, judging from the existence of systems such as HD181068 (Derekas et al. 2011) and KOI-126 (Feiden, Chaboyer & Dotter 2011), and theoretical modelling by means of adding TTs to existing triple star evolution codes (e.g. Toonen, Hamers & Portegies Zwart 2017) may also shed further light on this phenomenon that we know so little about, but such endeavours will be the contents of a future paper.

ACKNOWLEDGEMENTS

We thank a number of colleagues, including but not limited to Sverre Aarseth, Robert Izzard, Simon Jefferey, Philipp Podsiadlowski, Bo Wang, You Wu, Cong Yu, and Jilin Zhou, for discussion and encouragement.

This work was partly supported by the Natural Science Foundation of China (Grant Nos. 11521303, 11733008, 11390374), the Science and Technology Innovation Talent Programme of Yunnan Province (Grant No. 2017HC018), the Chinese Academy of Sciences (Grant No. KJZD-EW-M06-01), CIDMA strategic

project (UID/MAT/04106/2013), ENGAGE SKA (POCI-01-0145-FEDER-022217), and PHOBOS (POCI-01-0145-FEDER-029932), funded by COMPETE 2020 and FCT, Portugal.

REFERENCES

Abbott B. P. et al., 2016, PhRvL, 116, 061102
Correia A. C. M., Rodríguez A., 2013, ApJ, 767, 128
Correia A. C. M., Boué G., Laskar J., Rodríguez A., 2014, A&A, 571, A50
Correia A. C. M., Boué G., Laskar J., 2016, CeMDA, 126, 189
Counselman C. C., III, 1973, ApJ, 180, 307
Cuntz M., 2014, ApJ, 780, 14
Derekas A. et al., 2011, Science, 332, 216
Dong S., Katz B., Kushnir D., Prieto J. L., 2015, MNRAS, 454, L61
Eggleton P. P., 1973, MNRAS, 163, 279
Eggleton P. P., 1983, ApJ, 268, 368
Eggleton P. P., Kiseleva L. G., Hut P., 1998, ApJ, 499, 853
Fabrycky D., Tremaine S., 2007, ApJ, 669, 1298
Feiden G. A., Chaboyer B., Dotter A., 2011, ApJ, 740, L25
Fuller J., Derekas A., Borkovits T., Huber D., Bedding T. R., Kiss L. L., 2013, MNRAS, 429, 2425
Goldreich P., Keeley D. A., 1977, ApJ, 211, 934
Goodman J., Oh S. P., 1997, ApJ, 486, 403
Hamers A. S., Pols O. R., Claeys J. S. W., Nelemans G., 2013, MNRAS, 430, 2262
Han Z., Podsiadlowski P., 2004, MNRAS, 350, 1301
Hillel S., Schreier R., Soker N., 2017, MNRAS, 471, 3456
Hut P., 1981, A&A, 99, 126
Kiseleva L. G., Eggleton P. P., Mikkola S., 1998, MNRAS, 300, 292
Kozai Y., 1962, AJ, 67, 591
Kumar P., Goodman J., 1996, ApJ, 466, 946
Lidov M. L., 1962, P&SS, 9, 719
Mardling R. A., 1995, ApJ, 450, 722
Mardling R. A., 1995, ApJ, 450, 732
Mathis S., Auclair-Desrotour P., Guenel M., Gallet F., Le Poncin-Lafitte C., 2016, A&A, 592, A33
Musielak Z. E., Cuntz M., Marshall E. A., Stuit T. D., 2005, A&A, 434, 355
Ogilvie G. I., 2014, ARA&A, 52, 171
Pakmor R., Kromer M., Taubenberger S., Springel V., 2013, ApJ, 770, L8
Paxton B., Bildsten L., Dotter A., Herwig F., Lesaffre P., Timmes F., 2011, ApJS, 192, 3
Penev K., Sasselov D., Robinson F., Demarque P., 2007, ApJ, 655, 1166
Penev K., Sasselov D., Robinson F., Demarque P., 2009, ApJ, 704, 930
Peters P. C., 1964, PhRv, 136, 1224
Pols O. R., Tout C. A., Eggleton P. P., Han Z., 1995, MNRAS, 274, 964
Press W. H., Teukolsky S. A., 1977, ApJ, 213, 183
Ragazzo C., Ruiz L. S., 2017, CeMDA, 128, 19
Rebassa-Mansergas A., Rybicka M., Liu X.-W., Han Z., García-Berro E., 2015, MNRAS, 452, 1637
Rodriguez C. L., Haster C.-J., Chatterjee S., Kalogera V., Rasio F. A., 2016, ApJ, 824, L8
Sana H. et al., 2012, Science, 337, 444
Seidov Z. F., Skvirsky P. I., 2000, astro, preprint (arXiv:astro-ph/0003064)
Shappee B. J., Thompson T. A., 2013, ApJ, 766, 64
Thompson T. A., 2011, ApJ, 741, 82
Tokovinin A. A., 1997, A&AS, 124, 75
Tokovinin A., 2008, MNRAS, 389, 925
Toonen S., Hamers A., Portegies Zwart S., 2017, AAS, 229, 326.05
Torres G., Guenther E. W., Marschall L. A., Neuhäuser R., Latham D. W., Stefanik R. P., 2003, AJ, 125, 825
Tuchman Y., Sack N., Barkat Z., 1978, ApJ, 219, 183
Webbink R. F., 1984, ApJ, 277, 355
Whelan J., Iben I., Jr, 1973, ApJ, 186, 1007
Yip K. L. S., Leung P. T., 2017, MNRAS, 472, 4965
Zahn J.-P., 1977, A&A, 57, 383
Zahn J.-P., 2005, ASPC, 333, 4

SUPPORTING INFORMATION

Supplementary data are available at *MNRAS* online.

Animated Figure

Please note: Oxford University Press is not responsible for the content or functionality of any supporting materials supplied by the authors. Any queries (other than missing material) should be directed to the corresponding author for the article.

APPENDIX A: THEORETICAL CALCULATIONS OF TTS UNDER IDEAL CONDITIONS

For a hierarchical triple undergoing TTs, if it were the case that the internal dissipation of m_3 is infinitely efficient (which it is not), all the energy stored in the difference in the self-gravitational potential energy of m_3 between states α and β (see Fig. 1) would be effectively dissipated. Therefore, the amount of energy extracted from the inner binary orbit between m_1 and m_2, during the time it takes for the system to evolve from state α to state β, must be the same as the self-gravitational potential energy difference of m_3. As the system evolves back and forth twice between states α and β for every inner orbit, the rate of energy extraction from the inner orbit must equal four times this energy difference per inner orbital period.

How, then, should one calculate the difference in self-gravitational potential energy between the third body at states α and β? A spherical, perfectly homogeneous elastic body under the influence of a tidal force will assume the geometric shape of an ellipsoid. The self-gravitational potential energy of a homogeneous triaxial ellipsoid can be calculated from the equations given in Seidov & Skvirsky (2000), repeated below:

$$E_{\rm P} = \frac{3}{10} G M^2 \int_0^{+\infty} \frac{{\rm d}s}{Q_{\rm s}}, \qquad Q_{\rm s} = \sqrt{(a_x{}^2 + s)(a_y{}^2 + s)(a_z{}^2 + s)}. \tag{A1}$$

Here, W is the potential energy, a_x, a_y, and a_z are the semi-axes of the ellipsoid along the x, y and z axes, respectively, and M is the mass of the body. Thus, the potential energy difference between states α and β is simply

$$\Delta E_{\rm P} = \frac{3}{10} G M^2 \int_0^{+\infty} \left(\frac{1}{Q_\alpha} - \frac{1}{Q_\beta}\right) {\rm d}s. \tag{A2}$$

However, this treatment has the inconvenience that it is difficult to modify for an inhomogeneous ellipsoid, which is something we have to address later in this section. Therefore, we adopt a different approach, as follows.

Under the influence of a small geometrical distortion, which is true in our case, the ellipsoid resulting from the aforementioned homogeneous spherical body is still roughly spherical in shape. Adopting a spherical coordinate system (r, ψ, ξ) where $\psi = 0$ along the direction pointing towards the COM of the inner binary, the difference of the self-gravitational potential energy, between the initial sphere and that of the ellipsoid resulting from tidal influence, is simply the potential energy difference due to the change in radius at every (ψ, ξ), integrated over the surface of the sphere. Further assuming that the density difference of the body before and after applying the tidal force is negligible, the gravitational potential energy difference at (ψ, ξ) is equal to $(|\Delta R(\psi, \xi)|\rho g) \times (\frac{1}{2}|\Delta R(\psi, \xi)|)$, and

the integral of this over the entire surface of the sphere is

$$E_{\mathrm{P,ell}} - E_{\mathrm{P,sph}} = \int_0^{2\pi}\int_0^{\pi} (|\Delta R(\psi,\xi)|\rho g) \left(\frac{1}{2}|\Delta R(\psi,\xi)|\right) R_3^2 \sin\psi \mathrm{d}\psi \mathrm{d}\xi. \tag{A3}$$

Here, $E_{\mathrm{P,\,ell}}$ and $E_{\mathrm{P,\,sph}}$ are the potential energies of the body when it is a homogeneous ellipsoid and a homogeneous sphere, respectively; $|\Delta R(\psi,\xi)|$ is the absolute value of the change in radius at (ψ,ξ), $(|\Delta R(\psi,\xi)|\rho g)$ is the amount of mass displaced at (ψ,ξ) due to the change in radius, $(\frac{1}{2}|\Delta R(\psi,\xi)|)$ is the displacement of the centre of mass of the displaced mass, R_3 is the radius of the original sphere, and $R_3^2 \sin\psi$ is the Jacobian determinant for spherical integration. The general expression for $\Delta R(\psi,\xi)$ can be derived from

$$\Delta R(\psi,\xi) = R(\psi,\xi) - R_3, \quad R(\psi,\xi) = R_3[1 + \frac{5}{3}k_2\zeta P_2(\cos\psi)], \tag{A4}$$

where k_2 is the Love number, which is equal to 3/2 for a homogeneous fluid body, ζ is a parameter reflecting the magnitude of the tidal effects, the value of which we will deal with later in this section, and $P_2(\cos\psi)$ is a Legendre polynomial, equal to $\frac{1}{2}(3\cos^2\psi - 1)$. Since all stars are fluid bodies, we set $k_2 = \frac{3}{2}$ for a homogeneous body, and since $R(\psi,\xi)$ does not explicitly contain ξ, equation (A4) thus becomes

$$\Delta R(\psi,\xi) = \Delta R(\psi) = \frac{5}{4}R_3\zeta(3\cos^2\psi - 1), \tag{A5}$$

and, by extension, equation (A3) can be calculated by substituting the expressions for ρ and g, as well as equation (A5), to be

$$\begin{aligned} E_{\mathrm{P,ell}} - E_{\mathrm{P,sph}} &= \int_0^{2\pi}\int_0^{\pi} \frac{1}{2}\rho g(\Delta R(\psi))^2 {R_3}^2 \sin\psi \mathrm{d}\psi \mathrm{d}\xi \\ &= \int_0^{2\pi}\int_0^{\pi} \frac{1}{2}\left(\frac{m_3}{\frac{4}{3}\pi {R_3}^3}\right)\left(\frac{Gm_3}{{R_3}^2}\right) \left(\frac{5}{4}R_3\zeta(3\cos^2\psi - 1)\right)^2 {R_3}^2 \sin\psi \mathrm{d}\psi \mathrm{d}\xi \\ &= \frac{75}{128\pi}\frac{Gm_3^2\zeta^2}{R_3}\int_0^{2\pi}\int_0^{\pi}(3\cos^2\psi - 1)^2 \sin\psi \mathrm{d}\psi \mathrm{d}\xi. \end{aligned} \tag{A6}$$

Since

$$\int (3\cos^2 x - 1)^2 \sin x \mathrm{d}x = -\frac{9}{5}\cos^5 x + 2\cos^3 x - \cos x, \tag{A7}$$

the previous equation becomes

$$\begin{aligned} E_{\mathrm{P,ell}} - E_{\mathrm{P,sph}} &= \frac{75}{128\pi}\frac{Gm_3^2\zeta^2}{R_3}\int_0^{2\pi}\int_0^{\pi}(3\cos^2\psi - 1)^2 \sin\psi \mathrm{d}\psi \mathrm{d}\xi \\ &= \frac{75}{128\pi}\frac{Gm_3^2\zeta^2}{R_3}(2\pi)\frac{8}{5} \\ &= \frac{15}{8}\frac{Gm_3^2\zeta^2}{R_3}, \end{aligned} \tag{A8}$$

where G is the gravitational constant.

For a two-body tide, where one object experiences tidal force from the other, ζ is given by

$$\zeta = \frac{m_{\mathrm{per}}}{M}\left(\frac{R_0}{a}\right)^3, \tag{A9}$$

where m_{per} is the mass of the perturbing body, M is the mass of the perturbed body, R_0 is the spherical radius of the receiving body in the absence of tidal forces, and a is the distance between the two bodies. It follows that, in our situation, when $m = m_1 = m_2$, for states α and β (see Fig. 1 for definition),

$$\begin{aligned} \zeta_\alpha &= \left(\frac{a_2^3}{(a_2 + \frac{1}{2}a_1)^3} + \frac{a_2^3}{(a_2 - \frac{1}{2}a_1)^3}\right)\frac{m}{m_3}\left(\frac{R_3}{a_2}\right)^3 \\ \zeta_\beta &= \left[3\left(\frac{a_2}{\sqrt{a_2^2 + (\frac{1}{2}a_1)^2}}\right)^5 - \left(\frac{a_2}{\sqrt{a_2^2 + (\frac{1}{2}a_1)^2}}\right)^3\right]\frac{m}{m_3}\left(\frac{R_3}{a_2}\right)^3, \end{aligned} \tag{A10}$$

where a_1, a_2, m_1, m, and m_3 have already been defined in the text. Setting $u = (a_1/a_2)^2$, the above equations are strictly equivalent to

$$\begin{aligned} \zeta_\alpha &= \frac{m}{m_3}\left(\frac{R_3}{a_2}\right)^3 \frac{2 + \frac{3}{2}u}{\left(1 - \frac{1}{4}u\right)^3} \\ \zeta_\beta &= \frac{m}{m_3}\left(\frac{R_3}{a_2}\right)^3 \left[3\left(\frac{1}{1 + \frac{1}{4}u}\right)^{5/2} - \left(\frac{1}{1 + \frac{1}{4}u}\right)^{3/2}\right]. \end{aligned} \tag{A11}$$

When $a_1 << a_2$, it follows that u is small, and therefore terms of order u^2 and higher can be omitted:

$$\begin{aligned} \frac{2 + \frac{3}{2}u}{\left(1 - \frac{1}{4}u\right)^3} &= \left(2 + \frac{3}{2}u\right)\left(1 + \left(\frac{3}{4}u - \frac{3}{16}u^2 + \frac{1}{64}u^3\right)...\right) \\ &\sim \left(2 + \frac{3}{2}u\right)\left(1 + \frac{3}{4}u\right) \\ &\sim (2 + 3u) \\ \left(\frac{1}{1 + \frac{1}{4}u}\right)^{3/2} &= \left(1 - \frac{1}{4}u + \frac{1}{16}u^2...\right)^{3/2} \\ &\sim \left(1 - \frac{1}{4}u\right)^{3/2} \\ &= 1^{3/2} - (3/2)\frac{1}{4}u + \frac{1}{2}(3/4)\frac{1}{16}u^2... \\ &\sim \left(1 - \frac{3}{8}u\right) \\ \left(\frac{1}{1 + \frac{1}{4}u}\right)^{5/2} &\sim \left(1 - \frac{1}{4}u\right)^{5/2} \\ &\sim \left(1 - \frac{5}{8}u\right). \end{aligned} \tag{A12}$$

where '...' in each case denotes the use of a Taylor expansion. Substituting with these approximations, we arrive at

$$\begin{aligned} \zeta_\alpha &\sim \frac{2m}{m_3}\left(\frac{R_3}{a_2}\right)^3\left(1 + \frac{3}{2}\frac{a_1^2}{a_2^2}\right) \\ \zeta_\beta &\sim \frac{2m}{m_3}\left(\frac{R_3}{a_2}\right)^3\left(1 - \frac{3}{4}\frac{a_1^2}{a_2^2}\right). \end{aligned} \tag{A13}$$

Since $\frac{5}{2}\zeta$ is the magnitude of displacement at the surface of the third body at the points nearest and furthest to the binary system, it can be seen that the third body is still an approximate sphere despite the application of tidal forces.

Thus, combining equations (A8) and (A13), and comparing with equation (A2), we arrive at

$$\begin{aligned}\Delta E_{\rm P} &= E_{\rm P,ell,\alpha} - E_{\rm P,sph,\beta} \\ &= (E_{\rm P,ell,\alpha} - E_{\rm P,sph}) - (E_{\rm P,sph,\beta} - E_{\rm P,sph}) \\ &\sim \frac{135}{4}\frac{Gm^2R_3^5a_1^2}{a_2^8},\end{aligned} \tag{A14}$$

which is the difference in self-gravitational potential energy for the third body at equilibrium tide between states α and β for a homogeneous body. Note that, interestingly, it is invariant with the mass (or density) of the third body, and is a function of its radius only. This somewhat counterintuitive result is due to our previous assumptions that all tidal distortions are small – a smaller mass would result in a larger geometric distortion, and below a certain mass threshold (when $\zeta \sim 1$), our assumption of small distortion will simply cease to hold.

It should be noted that, in the derivations above, the third body is assumed to be homogeneous. When the mass of the third body is not homogeneously, but only spherically symmetrically, distributed, as is the case for many models of celestial bodies, the equation corresponding to equation (A3) is

$$\begin{aligned}E_{\rm P,ell} - E_{\rm P,sph} = &\int_0^{2\pi}\int_0^{\pi}\int_0^{R_3} |\Delta R(\psi, r)|\,(\rho(r) - \rho(r + {\rm d}r)) \\ &g(r)(\frac{1}{2}|\Delta R(\psi, r)|)r^2\sin\psi\,{\rm d}\psi\,{\rm d}\xi,\end{aligned}$$

where $\Delta R(\psi, r)$ is the vertical displacement of a point mass at (ψ, r), and the somewhat elusive dr (apparently missing at the end of the expression) is located in the $\rho(r + {\rm d}r)$ term. For example, for a body composed of an extremely compact central core and an outer envelope, with the core accounting for 60 per cent of its mass and the remaining mass being distributed in the envelope according to $\rho(r) = kr^{-1.5}$ (k is a constant),

$$\begin{aligned}E_{\rm P,ell} - E_{\rm P,sph} = &\int_0^{2\pi}\int_0^{\pi}\int_0^{R_3} |\Delta R(\psi, r)|\,(\rho(r) - \rho(r + {\rm d}r)) \\ &g(r)(\frac{1}{2}|\Delta R(\psi, r)|)r^2\sin\psi\,{\rm d}\psi\,{\rm d}\xi \\ = &\int_0^{2\pi}\int_0^{\pi}\int_{R_{\rm core}}^{R_3}\frac{1}{2}\Delta R^2(\psi, r) \\ &(\rho(r) - \rho(r + {\rm d}r))\,g(r)r^2\sin\psi\,{\rm d}\psi\,{\rm d}\xi \\ + &\int_0^{2\pi}\int_0^{\pi}\int_0^{R_{\rm core}}\frac{1}{2}\Delta R^2(\psi, r) \\ &(\rho(r) - \rho(r + {\rm d}r))\,g(r)r^2\sin\psi\,{\rm d}\psi\,{\rm d}\xi.\end{aligned} \tag{A16}$$

For a very small core, under the limit of when $R_{\rm core}$ goes to zero, the second term vanishes. To evaluate the first term, one should note that

$$\begin{aligned}\Delta R(\psi, r) &= \frac{5}{4}r\zeta(r)(3\cos^2\psi - 1), \\ \zeta(r) &= \zeta\frac{m_3}{m_3(<r)}\left(\frac{r}{R_3}\right)^3, \\ g(r) &= G\frac{m_3(<r)}{r^2},\end{aligned} \tag{A17}$$

where $\zeta(r)$ is the value of ζ corresponding to a radius r instead of the surface (i.e. $r = R_3$) of the perturbed body, and $m_3(<r)$ is the total mass included within a sphere of radius r centred at the centre of the perturbed body. It should also be noted that

$$\begin{aligned}(\rho(r) - \rho(r + {\rm d}r)) &= kr^{-1.5} - k(r + {\rm d}r)^{-1.5} \\ &= kr^{-1.5} - kr^{-1.5}\left(1 + \frac{{\rm d}r}{r}\right)^{-1.5} \\ &= kr^{-1.5} - kr^{-1.5}\left(1 - \frac{3}{2}\frac{{\rm d}r}{r}\right) \\ &= \frac{3}{2}kr^{-2.5}{\rm d}r,\end{aligned} \tag{A18}$$

and consequently

$$\begin{aligned}E_{\rm P,ell} - E_{\rm P,sph} = &\int_0^{2\pi}\int_0^{\pi}\int_0^{R_3} |\Delta R(\psi, r)|\,(\rho(r) - \rho(r + {\rm d}r)) \\ &g(r)(\frac{1}{2}|\Delta R(\psi, r)|)r^2\sin\psi\,{\rm d}\psi\,{\rm d}\xi \\ = &\lim_{R_{\rm core}\to 0}\int_0^{2\pi}\int_0^{\pi}\int_{R_{\rm core}}^{R_3}\frac{1}{2}\Delta R^2(\psi, r) \\ &(\rho(r) - \rho(r + {\rm d}r))\,g(r)r^2\sin\psi\,{\rm d}\psi\,{\rm d}\xi \\ = &\lim_{R_{\rm core}\to 0}\int_0^{2\pi}\int_0^{\pi}\int_{R_{\rm core}}^{R_3}\frac{1}{2}\frac{25}{16}r^2\zeta^2\left(\frac{m_3}{m_3(<r)}\right)^2 \\ &\left(\frac{r}{R_3}\right)^6(3\cos^2\psi - 1)^2\left(\frac{3}{2}kr^{-2.5}{\rm d}r\right)G\frac{m_3(<r)}{r^2} \\ &r^2\sin\psi\,{\rm d}\psi\,{\rm d}\xi \\ = &Gk\frac{75}{64}\lim_{R_{\rm core}\to 0}\int_0^{2\pi}\int_0^{\pi}\int_{R_{\rm core}}^{R_3} r^{-0.5}\zeta^2m_3^2\frac{1}{m_3(<r)} \\ &\left(\frac{r}{R_3}\right)^6(3\cos^2\psi - 1)^2\sin\psi\,{\rm d}r\,{\rm d}\psi\,{\rm d}\xi \\ = &Gk\frac{75}{64}\times\left(\int_0^{2\pi}{\rm d}\xi\right)\times\left(\int_0^{\pi}(3\cos^2\psi - 1)^2\sin\psi\,{\rm d}\psi\right) \\ &\times\left(\frac{\zeta^2m_3^2}{R_3^6}\right)\times\left(\lim_{R_{\rm core}\to 0}\int_{R_{\rm core}}^{R_3}\frac{r^{5.5}}{m_3(<r)}{\rm d}r\right) \\ = &Gk\frac{75}{64}\times(2\pi)\times\left(\frac{8}{5}\right)\times\left(\frac{\zeta^2m_3^2}{R_3^6}\right) \\ &\times\left(\lim_{R_{\rm core}\to 0}\int_{R_{\rm core}}^{R_3}\frac{r^{5.5}}{m_3(<r)}{\rm d}r\right) \\ = &\frac{15\pi}{4}k\frac{Gm_3^2\zeta^2}{R_3^6}\lim_{R_{\rm core}\to 0}\int_{R_{\rm core}}^{R_3}\frac{r^{5.5}}{m_3(<r)}{\rm d}r.\end{aligned} \tag{A19}$$

To proceed from here, we must ascertain the value of $m_3(<r)$ as a function of r, which is

$$\begin{aligned}m_3(<r) &= m_{3,\rm core} + m_{3,\rm envelope}(<r) \\ &= m_{3,\rm core} + \int_0^{2\pi}\int_0^{\pi}\int_{R_{\rm core}}^{r}\rho(\tilde{r})\tilde{r}^2\sin\psi\,{\rm d}\tilde{r}\,{\rm d}\psi\,{\rm d}\xi,\end{aligned} \tag{A20}$$

which, under the small $R_{\rm core}$ limit, can be calculated to be

$$\begin{aligned}m_3(<r) = &m_{3,\rm core} + \lim_{R_{\rm core}\to 0}\int_0^{2\pi}\int_0^{\pi}\int_{R_{\rm core}}^{r} \\ &\rho(\tilde{r})\tilde{r}^2\sin\psi\,{\rm d}\tilde{r}\,{\rm d}\psi\,{\rm d}\xi \\ = &\frac{3}{5}m_3 + \lim_{R_{\rm core}\to 0}\int_0^{2\pi}\int_0^{\pi}\int_{R_{\rm core}}^{r} \\ &\left(k\tilde{r}^{-1.5}\right)\tilde{r}^2\sin\psi\,{\rm d}\tilde{r}\,{\rm d}\psi\,{\rm d}\xi \\ = &\frac{3}{5}m_3 + 4\pi k\lim_{R_{\rm core}\to 0}\int_{R_{\rm core}}^{r}\tilde{r}^{0.5}{\rm d}\tilde{r} \\ = &\frac{3}{5}m_3 + \frac{8\pi}{3}kr^{1.5}.\end{aligned} \tag{A21}$$

Substituting equation (A21) back into equation (A19),

$$\begin{aligned}E_{\rm P,ell} - E_{\rm P,sph} = &\frac{15\pi}{4}k\frac{Gm_3^2\zeta^2}{R_3^6} \\ &\int_0^{R_3}\frac{r^{5.5}}{(3/5)m_3 + (8\pi/3)kr^{1.5}}{\rm d}r.\end{aligned} \tag{A22}$$

To calculate this integral, we carry out a numerical integration as follows. Setting $G = 1$, $m_3 = 1$, $\zeta = 1$, and $R_3 = 1$, whereupon $k = \frac{3}{20\pi}$,

$$\begin{aligned} E_{\rm P,ell} - E_{\rm P,sph} &= \frac{15\pi}{4} k \frac{G m_3^2 \zeta^2}{R_3^6} \int_0^{R_3} \frac{r^{5.5}}{(3/5)m_3 + (8\pi/3)kr^{1.5}} {\rm d}r \\ &= \frac{15\pi}{4} \frac{3}{20\pi} \int_0^1 \frac{r^{5.5}}{(3/5) + (2/5)r^{1.5}} {\rm d}r \\ &= 0.5625 \times \int_0^1 \frac{x^{5.5}}{0.6 + 0.4x^{1.5}} {\rm d}x \\ &= 0.0940, \end{aligned} \tag{A23}$$

and hence

$$\begin{aligned} E_{\rm P,ell} - E_{\rm P,sph} &= \frac{15\pi}{4} k \frac{G m_3^2 \zeta^2}{R_3^6} \int_0^{R_3} \frac{r^{5.5}}{\frac{3}{5}m_3 + \frac{8\pi}{3}kr^{1.5}} {\rm d}r \\ &\sim \frac{1}{20} \left(\frac{15}{8} \frac{G m_3^2 \zeta^2}{R_3} \right). \end{aligned} \tag{A24}$$

The density distribution used in the example above is typical of a red giant. Admittedly, real red giant internal density distributions are much more complicated (e.g. Tuchman, Sack & Barkat 1978), but since the final result is not too sensitive to the index, this is presumably not too bad an approximation. In other words, using a realistic density distribution for m_3 will induce a decrease of the self-gravitational potential energy difference, by about an order of magnitude. It can likewise be demonstrated that the final result is not very sensitive to the index of r involved. Again, as with a homogeneous body, the total mass of the receiving body is irrelevant to the result as long as $\zeta \ll 1$, since the m_3^2 term is cancelled out by the ζ^2 term.

It should be noted that these calculations establish only a very generous upper limit of the energy extraction rate of TTs, and should only be regarded as an order-of-magnitude estimate of how close a triple system needs to be for TTs to be non-negligible; for an exact calculation, please refer to our Stage 1 simulations in Section2.

APPENDIX B: TIDAL POTENTIAL FOR TTS

The gravitational potential of the tertiary is given by expression (20). Assuming that the shape of the tertiary only departs from a perfect sphere due to the tides raised by m_1 and m_2, the gravity field coefficients are solely given by the equilibrium tide contribution, i.e. $J_2 = J_2^t$, $C_{22} = C_{22}^t$, and $S_{22} = S_{22}^t$ (equation (32)). The gravitational potential for coplanar orbits is thus given by

$$V(\boldsymbol{r}) = -\frac{G m_3}{r} + V_1(\boldsymbol{r}) + V_2(\boldsymbol{r}), \tag{B1}$$

where $V_i(\boldsymbol{r})$ is the partial contribution of the mass m_i

$$\begin{aligned} V_i(\boldsymbol{r}) &= -\frac{G m_3 R_3^2}{2r^3} \left[k_2 \frac{m_i}{2m_3} \left(\frac{R_3}{r_i} \right)^3 \right] \\ &\quad - \frac{3G m_3 R_3^2}{r^3} \left[\frac{k_2}{4} \frac{m_i}{m_3} \left(\frac{R_3}{r_i} \right)^3 \cos 2\gamma_i \right] \cos 2\gamma \\ &\quad + \frac{3G m_3 R_3^2}{r^3} \left[-\frac{k_2}{4} \frac{m_i}{m_3} \left(\frac{R_3}{r_i} \right)^3 \sin 2\gamma_i \right] \sin 2\gamma \\ &= -\frac{G m_3}{r} \left[k_2 \zeta_i \left(\frac{R_3}{r} \right)^2 P_2(\cos(\gamma_i - \gamma)) \right], \end{aligned} \tag{B2}$$

with

$$\zeta_i = \frac{m_i}{m_3} \left(\frac{R_3}{r_i} \right)^3. \tag{B3}$$

For $\boldsymbol{r}$ in the orbital plane, we additionally have

$$\cos(\psi_i - \psi) = \cos(\gamma_i - \gamma) \tag{B4}$$

and we can rewrite the gravitational potential (B1) as

$$V(\boldsymbol{r}) = -\frac{G m_3}{r} \left[1 + k_2 \zeta \left(\frac{R_3}{r} \right)^2 P_2(\cos\psi) \right]. \tag{B5}$$

For a single perturber, for instance m_1, we have $\zeta = \zeta_1$ and $\psi_1 = 0$, so expression (B5) gives the usual tidal potential (since $m_2 = 0 \Rightarrow \zeta_2 = 0$). For two perturbers, ζ depends on the relative position of these perturbers with respect to the tertiary, and so we have

$$\zeta\, P_2(\cos\psi) = \zeta_1 P_2(\cos(\psi_1 - \psi)) + \zeta_2 P_2(\cos(\psi_2 - \psi)). \tag{B6}$$

To simplify things, we can approximate m_3 as an ellipsoid with its singular bulge constantly pointed towards the inner binary COM. In other words, we assume that the respective tidal bulges raised by m_1 and m_2 can be approximated to coalesce to from a single set of bulges, equal to that raised by a point mass at the COM of the inner binary. In this scenario, we only need to find the value of ζ for any value of ψ in order to find the ζ that characterizes the deformation of the entire m_3, regardless of ζ. Therefore, setting $\psi = 0$, and noting that $m = m_1 = m_2$, we have

$$\begin{aligned} \zeta &= \zeta_1 P_2(\cos\psi_1) + \zeta_2 P_2(\cos\psi_2) \\ &= \frac{m}{m_3} \left(\frac{R_3}{r_1} \right)^3 P_2(\cos\psi_1) + \frac{m}{m_3} \left(\frac{R_3}{r_2} \right)^3 P_2(\cos\psi_2) \\ &= \left[\frac{P_2(\cos\psi_1)}{(r_1/a_2)^3} + \frac{P_2(\cos\psi_2)}{(r_2/a_2)^3} \right] \frac{m}{m_3} \left(\frac{R_3}{a_2} \right)^3, \end{aligned} \tag{B7}$$

which is exactly equation (3).

This paper has been typeset from a TEX/LATEX file prepared by the author.